Light-by-light scattering in ultraperipheral collisions of heavy ions with future FoCal and ALICE 3 detectors

Antoni Szczurek
Institute of Nuclear Physics, PAN, Kraków
ul Radzikowskiego 152, PL-31-342 Kraków, Poland and
Rzeszów University
ul. Pigonia 1, PL-35-310 Rzeszów, Poland

I present possible future studies of light-by-light scattering using FoCal@ALICE and ALICE 3 detectors. Different mechanisms are discussed. The PbPb→PbPb$\gamma\gamma$ cross section is calculated within equivalent photon approximation in the impact parameter space. Several differential distributions are presented and discussed. We predict cross section in the (mb-b) range for typical ALICE 3 cuts, a few orders of magnitude larger than for the current ATLAS or CMS experiments. We also consider the two-π^0 background which can, in principle, be eliminated at the new kinematical range for the ALICE 3 measurements by imposing dedicated cuts on diphoton transverse momentum and/or so-called vector asymmetry.

DOI: https://doi.org/10.17161/758g5k69
Keywords: photon-photon scattering, ultrarelativistic heavy-ion processes, equivalent photon approximation, ALICE-3

1 Introduction

Photon-photon scattering is purely quantal effect (does not happen in classical physics). It was studied experimentally only recently in ultrarelativistic heavy ion collisions by the ATLAS [1] and CMS [2] collaborations. The ATLAS and CMS kinematics implies that box diagrams are the dominant reaction mechanism and other mechanisms are practically negligible. In [3] we studied whether this process could be sudied at lower photon-photon energies using ALICE and LHCb infrastructures. The experimental analysis using ALICE data is in progress. At the lower energies one should worry about background due to $\gamma\gamma \to \pi^0\pi^0$ process. We have worked out there techniques how to reduce the unwanted background [3].

The $\gamma\gamma \to \gamma\gamma$ is also interesting in the context of searching for effects beyond Standard Model [7].

Recently we explored what future FoCal [8] and ALICE 3 [9] detectors could do in this respect [4]. A forward electromagnetic calorimeter is planned as an upgrade to the ALICE experiment for data-taking in 2027-2029 at the LHC. The FoCal will cover pseudorapidities range of $3.4 < \eta < 5.8$. Runs 5 and 6 will measure more than five times the present Pb-Pb luminosity. This increase of luminosity, in combination with improved detector capabilities, will enable the success of the physical program planned for ALICE 3. A significant feature of FoCal and ALICE 3 programs is the ability to measure photons in relatively low transverse momenta.

In our recent paper we have taken into account different mechanisms for photon-photon scattering: boxes, VDM-Regge, two-gluon exchanges, meson (resonance) contributions, see Fig.1.

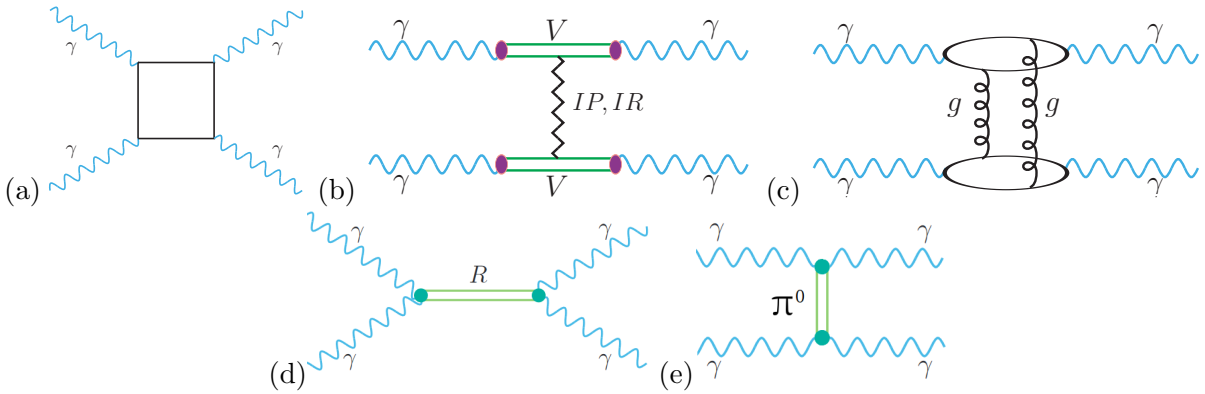

Figure 1 – Feynman diagrams representing different mechanisms: a) fermionic loops, b) VDM-Regge, c) 2-gluon exchange, d) low mass resonances in s-channel, e) π^0-exchange in t-channel.

Here, in this presentation, I will present the main results from [4].

2 Sketch of the formalism

Here we briefly discuss only some selected problems discussed in detail in [4].

2.1 Double-photon hadronic fluctuations

This component was calculated for the first time in [6] assuming vector dominance model. In this approach, the amplitude for the process is given as:

$$\begin{aligned}\mathcal{M} &= \Sigma_{i,j} C_i^2 C_j^2 \left(C_{I\!P} \left(\frac{s}{s_0}\right)^{\alpha_{I\!P}(t)-1} F(t) + C_{I\!R} \left(\frac{s}{s_0}\right)^{\alpha_{I\!R}(t)-1} F(t) \right) , \\ &+ \Sigma_{i,j} C_i^2 C_j^2 \left(C_{I\!P} \left(\frac{s}{s_0}\right)^{\alpha_{I\!P}(u)-1} F(u) + C_{I\!R} \left(\frac{s}{s_0}\right)^{\alpha_{I\!R}(u)-1} F(u) \right) . \end{aligned} \tag{1}$$

In the simplest version of the model $i,j = \rho^0, \omega, \phi$ (only light vector mesons are included). The couplings C_i, C_j describe the $\gamma \to V_{i/j}$ transitions that are calculated based on vector meson dilepton width. $C_{I\!P}$ and $C_{I\!R}$ are extracted from the Regge factorization hypothesis.

It was shown in [6] that the component is concentrated mainly at small photon transverse momenta which at not too small subsystem energies corresponds to $z \approx \pm 1$. The Regge trajectories are usually written in a linear form:

$$\begin{aligned}\alpha_{I\!P}(t/u) &= \alpha_{I\!P}(0) + \alpha'_{I\!P} t/u , \\ \alpha_{I\!R}(t/u) &= \alpha_{I\!R}(0) + \alpha'_{I\!R} t/u . \end{aligned} \tag{2}$$

These linear forms are valid at not too large $|t|$ or $|u|$. At large $|t|$ or $|u|$ the energy dependent factors are artificially small. In [4] we proposed to smoothly switch off the t/u dependent terms in (2) at $t, u \sim$ -0.5 GeV^2. The actual place where it should be done is not known precisely. Another option would be to use $\sqrt{t/u}$ trajectories [11,10].

We also analyzed in [4] whether more heavy vector mesons such as J/ψ can give a sizeable contribution.

For the double J/ψ fluctuations (both photons fluctuate into virtual J/ψ mesons) we took the following Ansatz for the helicity conserving amplitude:

$$\begin{aligned}\mathcal{M}^{J/\psi J/\psi}_{VDM} &= g^2_{J/\psi} C^{J/\psi}_{I\!P} \left(\frac{s}{s_0}\right)^{\alpha^{J/\psi J/\psi}_{I\!P}(t)-1} F^H_{J/\psi J/\psi I\!P}(t) F^H_{J/\psi J/\psi I\!P}(t) \\ &+ g^2_{J/\psi} C^{J/\psi}_{I\!P} \left(\frac{s}{s_0}\right)^{\alpha^{J/\psi J/\psi}_{I\!P}(u)-1} F^H_{J/\psi J/\psi I\!P}(u) F^H_{J/\psi J/\psi I\!P}(u) . \end{aligned} \tag{3}$$

In this case (double J/ψ fluctuations) only pomeron can be exchanged (no subleading reggeons are possible due to the pure $c\bar{c}$ structure of J/ψ). In this case, for simplicity, we took the simplified trajectories as

$$\alpha^{J/\psi J/\psi}_{I\!P}(t) = \alpha^{J/\psi J/\psi}_{I\!P}(u) = \alpha^{J/\psi J/\psi}_{I\!P}(0) . \tag{4}$$

Here the t/u dependencies of the trajectories are totally ignored. In numerical calculations we take $\alpha^{J/\psi J/\psi}_{I\!P}(0) = 1.3 - 1.4$ (typical hard pomeron). Since the J/ψ mesons are far off-mass-shell and more compact than light vector mesons the form factors are different than those for light vector mesons. In [4] we took them in the following form:

$$F^H_{J/\psi J/\psi I\!P}(t) = \exp\left(\frac{t - m^2_{J/\psi}}{\Lambda^2_{J/\psi}}\right) , \tag{5}$$

$$F^H_{J/\psi J/\Psi I\!P}(u) = \exp\left(\frac{u - m^2_{J/\psi}}{\Lambda^2_{J/\psi}}\right) . \tag{6}$$

These form factors are normalized to 1 on the meson (J/ψ) mass shell. One could also use monopole form factors in this context. The form factors reduce the $J/\psi J/\psi$ component of the amplitude in comparison

to light vector meson components. However, due to compactness of J/ψ we expect $\Lambda_{J/\psi}$ to be large. In [4]we took $\Lambda_{J/\psi} = 2$ GeV for illustration, the actual value is not precisely known. Also, the normalization parameter $C_{I\!P}^{J/\psi}$ is not well known. It is expected to be smaller than for light vector mesons.

In a similar fashion, one could include one J/ψ fluctuation and one light vector meson fluctuation. However, there the choice of trajectories is not clear. We will leave the discussion of these components for future studies.

In [4] we assumed the following helicity structure of the double photon hadronic fluctuation amplitude:

$$\mathcal{M}^{(t)}_{\lambda_1\lambda_2\to\lambda_3\lambda_4} = A(t)\,\delta_{\lambda_1\lambda_3}\delta_{\lambda_2\lambda_4}\,, \tag{7}$$

$$\mathcal{M}^{(u)}_{\lambda_1\lambda_2\to\lambda_3\lambda_4} = A(u)\,\delta_{\lambda_1\lambda_4}\delta_{\lambda_2\lambda_3}\,. \tag{8}$$

$A(t)$ and $A(u)$ are given explicitly in (1). Then the total double VDM amplitude, including t and u processes, reads:

$$\mathcal{M}^{VDM}_{\lambda_1\lambda_2\to\lambda_3\lambda_4} = \frac{1}{\sqrt{2}}\left(\mathcal{M}^{VDM,(t)}_{\lambda_1\lambda_2\to\lambda_3\lambda_4} + \mathcal{M}^{VDM,(u)}_{\lambda_1\lambda_2\to\lambda_3\lambda_4}\right)\,. \tag{9}$$

Now we can add amplitudes for different mechanisms:

$$\mathcal{M}_{\lambda_1\lambda_2\to\lambda_3\lambda_4} = \mathcal{M}^{boxes}_{\lambda_1\lambda_2\to\lambda_3\lambda_4} + \mathcal{M}^{VDM}_{\lambda_1\lambda_2\to\lambda_3\lambda_4} + \mathcal{M}^{\pi^0}_{\lambda_1\lambda_2\to\lambda_3\lambda_4} + \dots\,. \tag{10}$$

In the following, we shall discuss the sum of the larger two components (boxes and VDM) and quantify their interference effects.

2.2 Cross section for nuclear UPC

In [4] the nuclear cross section is calculated using equivalent photon approximation (EPA) in the b-space. In this approach, the diphoton cross section can be written as (see [6]):

$$\begin{aligned}\frac{d\sigma(PbPb\to PbPb\gamma\gamma)}{dy_{\gamma_1}dy_{\gamma_2}dp_{t,\gamma}} &= \int \frac{d\sigma_{\gamma\gamma\to\gamma\gamma}(W_{\gamma\gamma})}{dz}N(\omega_1,b_1)N(\omega_2,b_2)S^2_{abs}(b) \\ &\times\; d^2bd\bar{b_x}d\bar{b_y}\frac{W_{\gamma\gamma}}{2}\frac{dW_{\gamma\gamma}dY_{\gamma\gamma}}{dy_{\gamma_1}dy_{\gamma_2}dp_{t,\gamma}}dz\,,\end{aligned} \tag{11}$$

where $\bar{b}_x = (b_{1x}+b_{2x})/2$ and $\bar{b}_y = (b_{1y}+b_{2y})/2$. The relation between $\vec{b}_1$, $\vec{b}_2$ and impact parameter: $b = |\vec{b}| = \sqrt{|\vec{b}_1|^2 + |\vec{b}_2|^2 - 2|\vec{b}_1||\vec{b}_2|\cos\phi}$. Absorption factor $S^2_{abs}(b)$ in [4]was calculated as:

$$S^2_{abs}(b) = \Theta(b - b_{max}) \tag{12}$$

or

$$S^2_{abs}(b) = exp\left(-\sigma_{NN}T_{AA}(b)\right)\,, \tag{13}$$

where σ_{NN} is the energy-dependent nucleon-nucleon interaction cross section, and $T_{AA}(b)$ is related to the so-called nuclear thickness, $T_A(b)$,

$$T_{AA}\left(|\vec{b}|\right) = \int d^2\rho T_A\left(\vec{\rho}-\vec{b}\right)T_A\left(\rho\right), \tag{14}$$

and the nuclear thickness is obtained by integrating the nuclear density

$$T_A\left(\vec{\rho}\right) = \int \rho_A\left(\vec{r}\right)dz, \qquad \vec{r} = (\vec{\rho}, z)\,, \tag{15}$$

where ρ_A is the nuclear charge distribution. The nuclear photon fluxes $N(\omega_1, b_1)$ and $N(\omega_2, b_2)$ are calculated using realistic charge distribution.

Very often the UPC results are shown only with a sharp cut on the impact parameter, usually taken as a sum of two radii of the nuclei, i.e. $b > R_A + R_B \approx 14$ fm for Pb+Pb collisions. Due to the no homogeneous nuclear charge distribution, it seems to be more reasonable to use the absorption factor given by Eq. (13).

2.3 Background contribution

As shown in [3] the $\gamma\gamma \to \pi^0(\to 2\gamma)\pi^0(\to 2\gamma)$ reaction constitutes a background for the measurement of $\gamma\gamma \to \gamma\gamma$ process at intermediate $M_{\gamma\gamma}$.

In our approach the calculation of the background proceeds in three steps. First, the cross section for $\gamma\gamma \to \pi^0\pi^0$ is calculated (for details, see [12]). Next the cross section for $AA \to AA\pi^0\pi^0$ is computed in the equivalent photon approximation in an analogous way as described in the subsection above. In the last step the simulation of both π^0 decays is performed and joint distributions of one photon from the first π^0 and one photon from the second π^0 are constructed.

3 Selected results

3.1 Elementary cross section

In Fig. 2 we show $d\sigma/dz$ for $\gamma\gamma \to \gamma\gamma$ for (a) boxes, (b) double hadronic fluctuation calculated within the VDM-Regge approach and (c) the π^0-exchange calculated as in Ref. [5]. Results are presented for five energies in the range of $(1-50)$ GeV. At larger energies, the VDM-Regge contribution peaks at $z = \pm 1$. On the other hand, the π^0 exchange contribution has minima at $z = \pm 1$ which is due to the structure of corresponding vertices. The latter contribution is relatively small. In general, the box contributions dominate, especially for low photon-photon scattering energies. At larger scattering energies ($W_{\gamma\gamma} > 2$ GeV) the VDM-Regge contribution competes with the box contributions only at $z \sim \pm 1$. Can one expect sizeable interference effects of both mechanisms?

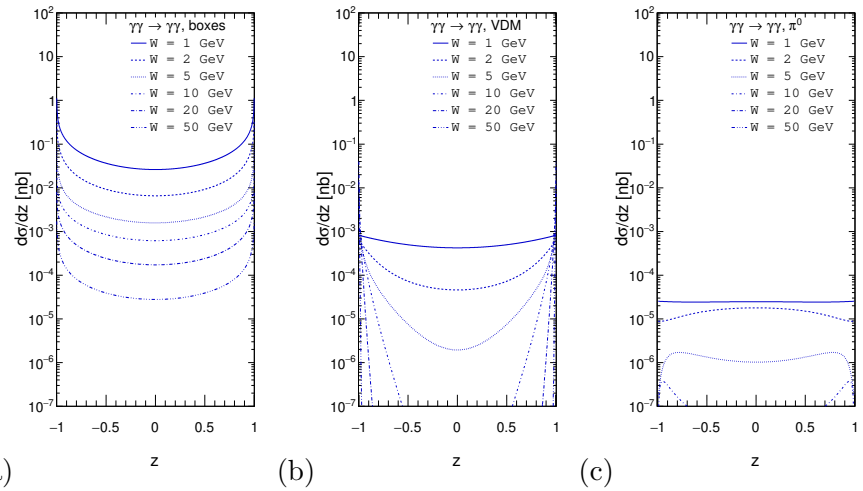

Figure 2 – $cos(\theta)$ distributions for (a) boxes, (b) double hadronic fluctuations and (c) π^0 exchange for different photon-photon collision energies $W = 1, 2, 5, 10, 20, 50$ GeV.

Now we wish to discuss briefly the second biggest contribution: double photon fluctuations. The results are shown in Fig.2. In [4] we includeed both light vector mesons ρ^0, ω, ϕ) as well as J/ψ (one or two) as described in the theoretical section. Our results, for two collision energies ($W = 2, 5$ GeV), are shown in Fig.3. The dotted line includes only light vector meson fluctuations, the dashed line in addition double J/ψ fluctuations and the solid line all combinations of photon fluctuations. The inclusion of J/ψ meson fluctuations leads to an enhancement of the cross section at -0.5 $< z <$ 0.5. The enhancement is more spectacular for larger collision energy. The corresponding cross section there is, however, much smaller than the box contribution (see Fig.2).

Now we wish to concentrate on how the elementary cross section changes when adding the box and VDM-Regge contributions. This is shown in Fig.4. The red line represents the incoherent sum, while the blue line includes also interference effects. In this calculation, the so-called "sqrt" trajectories [10,11] were used. one observes a negative interference effect. Adding the remaining contributions would lead to additional deviations.

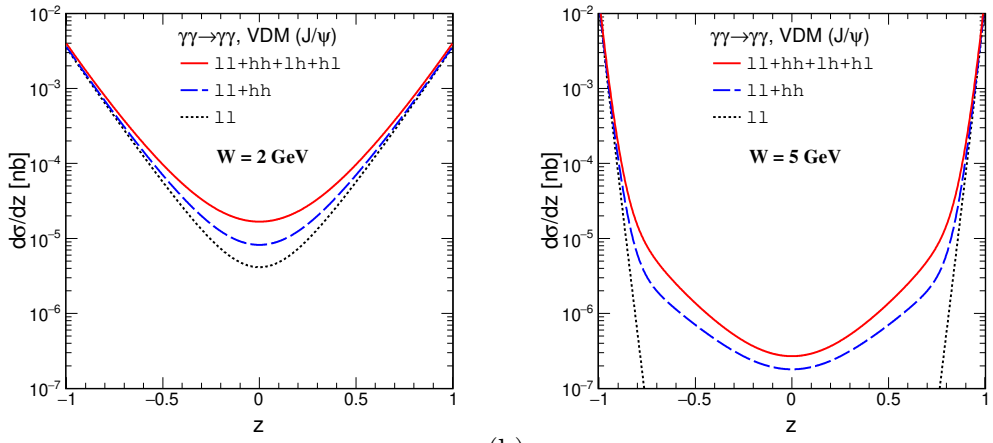

(a) (b)

Figure 3 – Modification of $d\sigma/dz$ due to inclusion of fluctuations of photons into virtual J/ψ mesons: (a) $W = 2$ GeV, (b) $W = 5$ GeV. The top solid line includes all components (light (l) and heavy (h) vector mesons), the dotted line only light vector mesons.

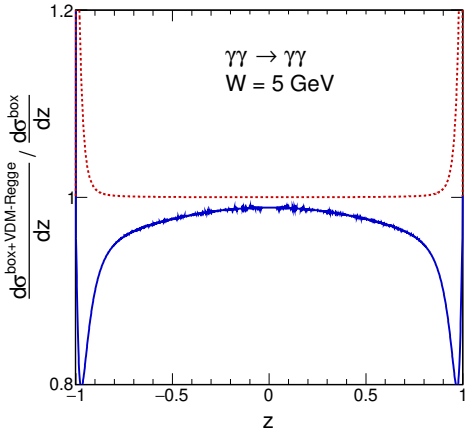

Figure 4 – The ratio of the coherent (blue) and incoherent (red) sum of the box and VDM-Regge contributions divided by the cross section for the box contribution alone for $W = 5$ GeV.

3.2 Heavy ion UPC

To summarize the present status of $\gamma\gamma \to \gamma\gamma$ scattering in Fig.3.2 we confront results of our calculation with current ATLAS data [13]. We discuss also how the results depend on the treatment of absorption corrections. The results of the two different approximations (as described in the figure caption) almost coincide. For comparison, we show also results obtained with the SuperChic generator [14]. In general, there is reasonable agreement of the Standard Model predictions with the ATLAS data. Similar agreement is achieved for the CMS data.

Many light vector mesons have large coupling to two photons. In [5] for a first time the role of resonances was discussed, for elementary cross section only. In Fig.6 we show the contributions of light mesonic photon-photon resonances for heavy ion UPC. The results shown are for a broad range of photon rapidities and transverse momenta. We show distribution in diphoton inariant mass (left) and photon transverse momentum (right). It is obvious that elimination of the resonance contributions may be difficult. But perhaps it is not necessary as the mesonic resonance contributions are a part of photon-photon scattering. The cuts used by ATLAS or CMS allowed to eliminate the contributions of light mesons. The contribution of heavy mesons is expected to be small.

The FoCal detector planned for Run 4 was described in [8]. It is a general purpose detector. It can also measure photons. We start our presentation from the results when both photons are measured by FoCal. In Fig.7 (a) we show results when both photons have energies bigger than 200 MeV. In addition, we show the contribution of the $\pi^0\pi^0$ background. In this case, only two photons are measured. Without

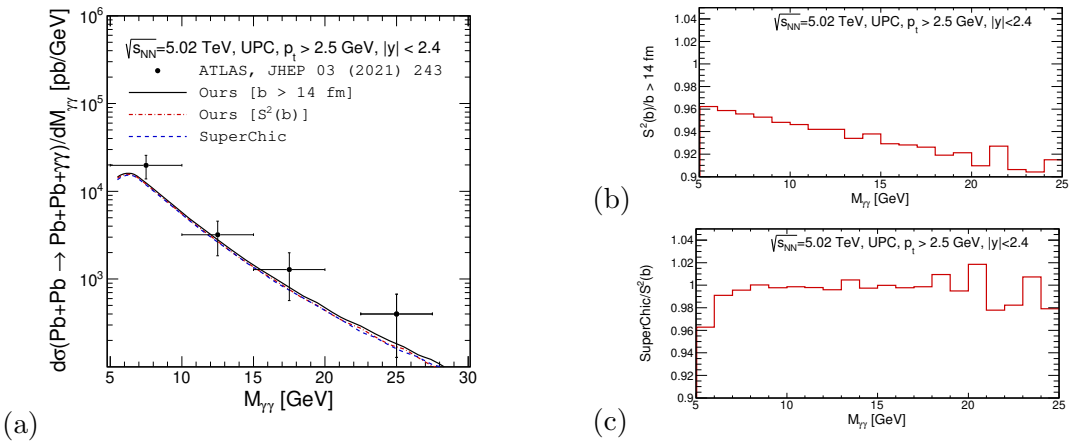

Figure 5 – Differential cross section as a function of two-photon invariant mass at $\sqrt{s_{NN}} = 5.02$ TeV. (a) The ATLAS experimental data are collected together with theoretical results including a sharp cut on impact parameter ($b > 14$ fm - solid black line) and smooth nuclear absorption factor $S^2(b)$ (dash-dotted red line). For completeness, results that are obtained with the help of Eq. (11) are compared with results from SuperChic. The right panel shows two ratios: (b) ratio of distributions calculated by us with sharp and smooth cut-off on impact parameter and (c) the ratio of SuperChic result to our result, using a smooth representation of the gap survival factor.

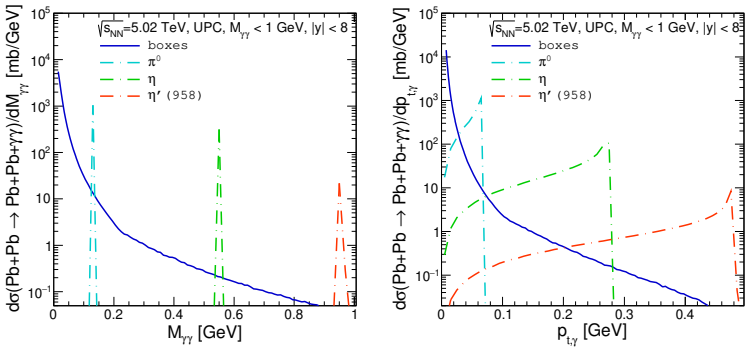

Figure 6 – Box versus resonance contributions for diphoton invariant mass (left) and photon transverse momentum (right).

additional cuts, the background is clearly bigger than the signal. However, by imposing extra conditions on vector asymmetry, we can lower the background contribution.

In Fig.8 we show similar distributions but for $p_t > 0.2$ GeV and combined ALICE and FoCal rapidity region. Here in some regions of the phase space, the VDM-Regge contribution could be seen as 10% modification of the cross section with respect to the calculations with only boxes. Here the separated VDM-Regge component is even bigger. We conclude that already at Run 4 one could indirectly observe a signature of mechanisms other than fermionic boxes.

Now we will show distributions relevant for the ALICE 3 detector.

In Fig. 9 we show distributions in diphoton invariant mass for photons $-4 < y_1, y_2 < 4$ and $E_\gamma > 50$ MeV (see Ref. [9]). We show the light-by-light box contribution (solid line) as well as the $\pi^0\pi^0$ background contribution (red lines). At diphoton invariant masses, 0.5 GeV $< M_{\gamma\gamma} <$ 1 GeV, the background contribution is almost as big as the signal contribution. As discussed in [3] it can be to some extent reduced. Although the background is smaller than fermionic boxes in the full range of diphoton invariant mass, it can be further reduced by imposing the cut on $|\vec{p_{1t}} + \vec{p_{2t}}| < 0.1$ GeV and vector asymmetry $A_V < 0.02$. Imposing a cut on the background causes that the background in the whole diphoton invariant mass range is much smaller than the signal.

In Fig. 10 we show distribution in $y_{diff} = y_1 - y_2$. Again different contributions are shown separately. The results for the double-π^0 background contribution are particularly interesting. It has a maximal contribution at $y_{diff} = 0$ and drops quickly for larger $|y_{diff}|$. An extra cut on y_{diff} could therefore considerably reduce the unwanted double-π^0 contribution. In Fig. 10 we show what happens when

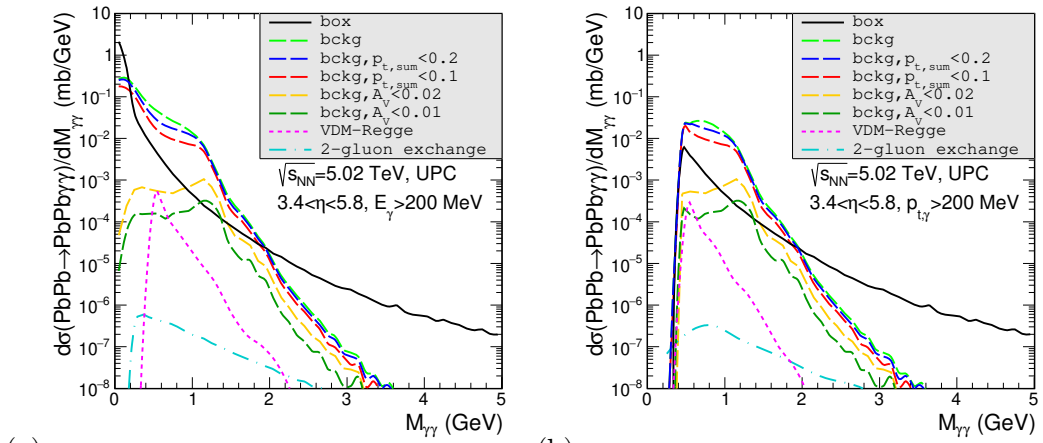

Figure 7 – Diphoton invariant mass distribution for the UPCs. Predictions are made for the future FoCal acceptance, i.e. (a) $E_{t,\gamma} > 200$ MeV and $3.4 < y_{\gamma_{1/2}} < 5.8$, (b) $p_{t,\gamma} > 200$ MeV and $3.4 < y_{\gamma_{1/2}} < 5.8$. Here, both photons are "measured" in FoCal. The background contribution is presented for different cuts.

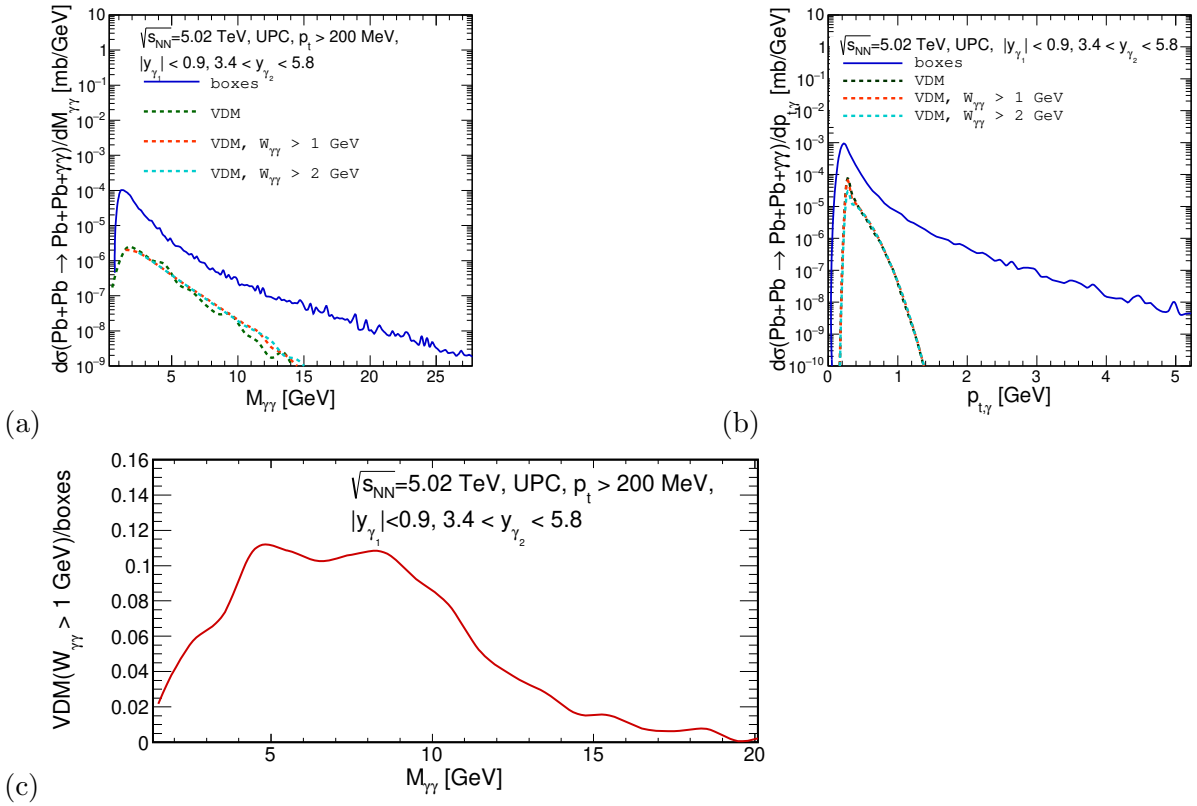

Figure 8 – Prediction for the FoCal detector in association with mid-rapidity ALICE detector for photons: $p_t > 200$ MeV, diphoton mass $M_{\gamma\gamma} > 400$ MeV and photon rapidities $|y_1| < 0.9$ and $y_2 \in (3.4, 5.8)$. The blue line corresponds to fermionic loops and the green lines to the VDM-Regge contribution. (a) Diphoton invariant mass distribution, (b) photon transverse momentum distribution, (c) ratio of the VDM-Regge ($W_{\gamma\gamma} > 1$ GeV) and box contributions as a function of di-photon invariant mass. No interference effects were included here.

imposing the cut on y_{diff}. The effect of such a cut on box contribution is relatively small but leads to a huge reduction of the $\pi^0\pi^0$ background. The effect of the cut is much larger for small $M_{\gamma\gamma}$ and therefore could be avoided if one is interested in this region of energies.

In Fig.11 we show distribution in $M_{\gamma\gamma}$ (a) and p_t (b) for a planned special photon detector in forward direction $3 < y_\gamma < 5$. Here $p_t > 5$ MeV was imposed as described in Ref. [9]. We show that at low $M_{\gamma\gamma}$ and low p_t the LbL signal by far exceeds the $\pi^0\pi^0$ background, even without including any suppression

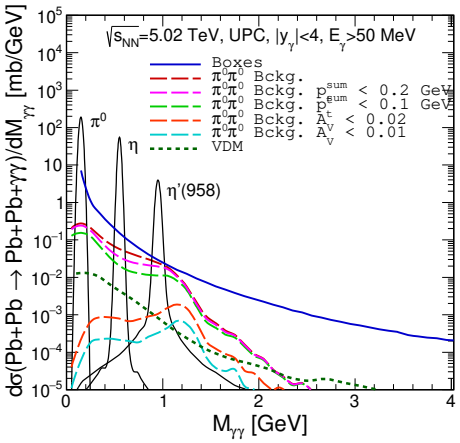

Figure 9 – Diphoton invariant mass distribution for ALICE 3, i.e. rapidity $y_{1/2} \in (-4, 4)$ and photon energy $E_\gamma >$ 50 MeV. Here the blue solid line relates to the box contribution, the dotted line to the VDM-Regge component and the dashed lines are for double-π^0 background contribution. Here we impose several extra conditions on diphoton transverse momenta and vector asymmetry.

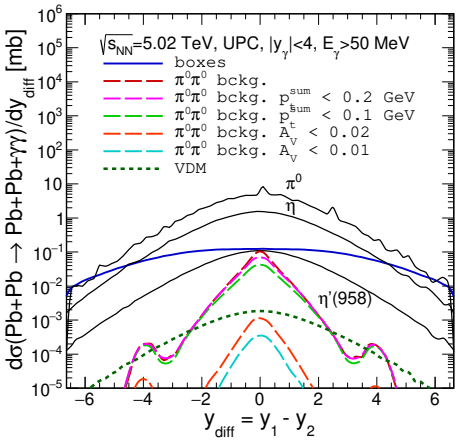

Figure 10 – Differential cross section as a function of $y_{diff} = y_1 - y_2$ for extended ALICE 3 kinematics: $|y_{1/2}| < 4$ and $E_\gamma > 50$ MeV. Results are presented for boxes, resonances, VDM-Regge and double-π^0 background.

condition for the background. Here we assumed 2 π azimuthal coverage of the planned special photon detector. The special detector having the planned very small transverse momentum coverage should allow to measure completely new, low energy, regime of photon-photon scattering. Here both background and mesonic resonance contributions should be absent.

4 Conclusions

Recently we discussed different mechanisms of $\gamma\gamma \to \gamma\gamma$ scattering such as leptonic/quarkish boxes, double hadronic fluctuations, neutral t/u-channel pion exchanges and two-gluon exchanges. Possible effects of the searched for subleading mechanisms have been discussed. The latter contributions turned out difficult to be identified in ATLAS and CMS measurements. We have discussed possible interference effect of box and double-hadronic fluctuations for $\gamma\gamma \to \gamma\gamma$ scattering for future measurements.

In the literature only the box contributions were discussed before. We have tried to identify the region where the other contributions could appear. In addition we discussed how to reduce the unwanted $\gamma\gamma \to \pi^0\pi^0$ background.

The FoCal project does not seem to allow for breakthroughs for LbL scattering. but may be used to supplement the ALICE, not yet officially presented, experimental studies.

We have also made predictions for the ALICE 3 ($-4 < y_\gamma < 4$) and for a planned special soft

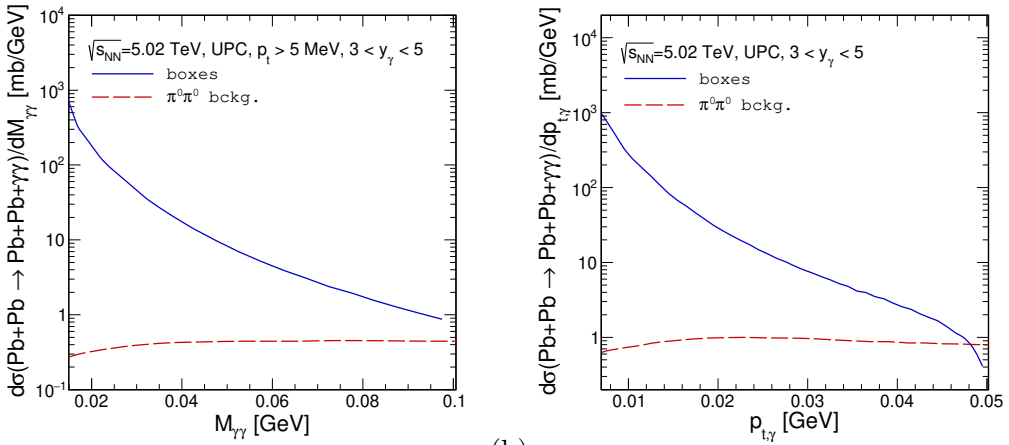

Figure 11 – Prediction for the ALICE 3 experiment for soft photons: $p_t = (5 - 50)$ MeV and photon rapidities $y_i \in (3, 5)$. The blue line corresponds to fermionic loops, the red line relates to the double-π^0 background. (a) diphoton invariant mass distribution, (b) photon transverse momentum distribution.

photon detector ($3 < y_\gamma < 5$). We have shown that by imposing a cut on $y_{diff} = y_1 - y_2$ one can efficiently eliminate the unwanted $\pi^0\pi^0$ background. The soft photon detector can be used to measure the $\gamma\gamma \to \gamma\gamma$ scattering at extremely small energies, $W_{\gamma\gamma} < 0.05$ GeV. Therefore we conclude that the ALICE 3 infrastructure will be extremely useful to study the $\gamma\gamma \to \gamma\gamma$ scattering in a new, not yet explored, domain of energies and transverse momenta. In this domain the $\pi^0\pi^0$ background can to large extent be eliminated.

In our recent calculations we used EPA in the impact parameter space. In the future one can try to use also so-called Wigner function approach used for e^+e^- production in semi-peripheral lead-lead collisions (never used for the di-photon production). This goes, however, beyond the scope of the first exploratory study.

5 Acknowledgments

This work was partially supported by the Polish National Science Center grant UMO-2018/31/B/ST2/03537 and by the Center for Innovation and Transfer of Natural Sciences and Engineering Knowledge in Rzeszów.

References

1. M. Aaboud et al. (ATLAS collaboration), Nature Phys. **13**, 852 (2017).
2. A.M. Sirunyan et al. (CMS collaboration), Phys. Lett. **B797**, 134826 (2019).
3. M. Klusek-Gawenda, R. McNulty,, R. Schicker and A. Szczurek, Phys. Rev. **D99**, 093013 (2019).
4. P. Jucha, M. Klusek-Gawenda and A. Szczurek, Phys. Rev. **D109**, 014004 (2024).
5. P. Lebiedowicz and A. Szczurek, Phys. Lett. **B772**, 330 (2017).
6. M. Klusek-Gawenda, P. Lebiedowicz and A. Szczurek, Phys. Rev. **C93**, 044907 (2016).
7. C. Baldenegro, S. Fichet, G. von Gersdorff and C. Royon, JHEP **06**, 131 (2018).
8. C. Loizides, W. Riegler et al. (ALICE collaboration), CERN Document Server (2020), 2211.024991.
9. L. Musa, W. Riegler et al. (ALICE collaboration), CERN Document Server (2022), 2211.02491.
10. M.M. Brisudova, L. Burakovsky and T. Goldman, Phys. Rev. **D61**, 054013 (2000).
11. M.M. Brisudova, L. Burakovsky, T. Goldman and A. Szczepaniak, Phys. Rev. **D67**, 094016 (2003).
12. M. Klusek-Gawenda and A. Szczurek, Phys. Rev. **C87**, 054908 (2013).
13. G. Aad et al. (ATLAS collaboration), Phys. Rev. Lett. **123**, 052001 (2019).
14. L.A. Harland-Lang, M. Tasevsky, V.A. Khoze and M.G. Ryskin, Eur. Phys.J. **C80**, 925 (2020).